MAGNETIC BEHAVIOR OF Gd-RICH SPIN-GLASS SYSTEMS

by

ABDEL-LATIF AL-SHARIF

B.Sc., YARMOUK UNIVERSITY-JORDAN, 1984

A MASTER'S THESIS

submitted in partial fulfilllment of the

requirement for the degree

MASTER OF SCIENCE

Department of physics

KANSAS STATE UNIVERSITY

Manhattan, Kansas

1988

Approved by:

Michael J. Sutton

Major Professor

ACKNOWLEDGEMENT

I thank God Almighty (ALLAH) for giving me the strength to continue this work.

I would like to express my most sincere gratitude to Dr. M. J. O'Shea for his guidance and encouragement throughout the course of this work.

I thank my parents for their love and my wife Suhad for her encouragment and care.

I thank Dr. M. J. O'Shea and Dr. A. Fert for providing me with the torque data.

I thank Dr. G. Hadjipanayis for letting us use some of his apparatus.

I thank Dr. D. Dragsdorf for the use of x-ray apparatus.

I thank Dr. D. J. Sellmyer at university of Nebraska at Lincoln for the use of the splat-cooling apparatus.

I extend thanks to my committee members Dr. N. Folland and Dr. G. Hadjipanayis.

I acknowledge the financial support of M'utah University-Jordan.

TABLE OF CONTENTS

List Of Figures

CH.I

INTRODUCTION

1.1 Objective Of Work

Many amorphous [1,2] and disordered crystalline alloys [3,4] show a paramagnetic (PM) to spin-glass (SG) phase transition with decreasing temperature. In the SG phase the spins are frozen in random directions. If the composition of the alloy is changed then in many cases double-transition behavior, that is a PM to ferromagnetic (FM) to SG sequence of transitions, can be observed [1-4]. The signatures of a SG transition are (i) a decrease in the ac susceptibility (ii) onset of hysteresis (iii) a time dependence of magnetization which has a maximum decay rate at intermediate temperatures (chapt. VI).

In this work we shall take an alloy showing double transition behavior ($Gd_{72}Ga_{18}B_{10}$) and alloy with a number of elements both magnetic and non-magnetic. The purpose of this work is to gain a better understanding of the properties of these alloy systems which are important in producing double transition behavior.

1.2 Introduction

The magnetic phase diagram of an amorphous Gd alloy system with double transition behavior is shown in figure 1.1. It is currently believed that the essential ingredient

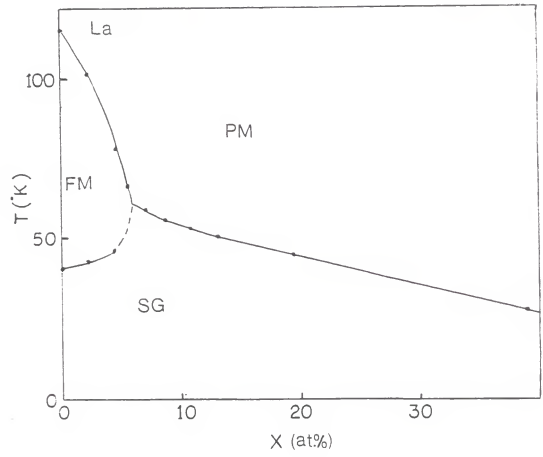

Figure 1.1 The magnetic phase diagram of the $Gd_{72-l}La_lGa_{18}B_{10}$.

required to produce such behavior is a random component in the microscopic exchange interactions [5,6,7]. Although mean field models with random exchange interactions are able to reproduce this phase diagram [8], more realistic models with short-range interactions are only able to reproduce PM-SG transition behavior [9]. The double transition behavior however has not so far been produced in any short-range model. The effect of exchange fluctuations can also be seen in high field magnetization measurments where the magnetization shows a slow approach to saturation because of the presence of antiferromagnetic interactions. Examples are shown in fig 1.2 for $(Gd\text{-}La)_{72}Ga_{18}B_{10}$ alloys where for high La content only a PM-SG transition is present due to strong exchange fluctuations and the magnetization approaches saturation slowly. It has been suggested that in addition to the exchange some anisotropy is also required [9,10] and it has been shown that anisotropy is required to stabilize the SG behavior at low temperature in model systems where exchange fluctuations are present [7,9]. Such models have not so far reproduced the double-transition behavior.

A number of rare-earth amorphous alloys show a PM-speromagnetic (SM) transition with decreasing temperature [11,12,13]. The speromagnetic state is similar to the SG state in that the spins are frozen in random orientations

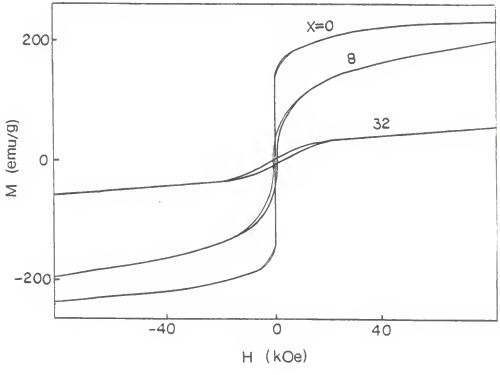

Figure 1.2 Hysteresis loops of the La system up to 80 kOe for the x=0, 8, and 32 samples. The arrows indicate the expected maggnetization for collinear alligment of the Gd spins.

but the freezing here is due only to the random magnetic anisotropy. Recently it has been shown that alloys with a small enough random magnetic anisotropy (but large compared to the anisotropy present in transition metal alloys) show behavior similar to double transition behavior with a series of PM-FM-SM transition with decreasing temperature [10]. In this work we shall study the magnetic properties of $Gd_{72-x}T_xGa_{18}B_{10}$ alloy where T is a transition metal or rare earth. The alloy with composition x=0, i.e. $Gd_{72}Ga_{18}B_{10}$, shows double-transition behavior and has been studied in some detail [2,14]. The purpose of this work is to dilute with the element T which can (i) be magnetic (Fe,Co,Mn,Er), (ii) be non-magnetic (La,Al,Th, Pd,Mo), (iii) incorporate negligible anisotropy (Fe, Co, Mn, La, Al, Th, Pd, Mo), (iv) incorporate a random magnetic anisotropy (Er) to gain a better understanding of how varying the microscopic interactions affect the double-transition behavior. We note that the La system was studied previously in some detail [15]. We shall also compare these results to the TM = Mn and Ni systems which were studied previously by Jantan [15]. Scaling in these alloys at the PM-FM and FM-SG transitions are consistent with these transitions being true phase transitions and not just a gradual freezing in of the spins.

CH. II

THEORETICAL ASPECTS

2.1 Introduction

For the 3d transition metals, the electronic configuration for an isolated atom is $(Ar)^{18}\ 3d^{n}\ 4s^{2}$ where n is the number of electrons in the 3d shell. In most alloys the d and s electrons are partialy delocalized and form a conduction band. The orbital angular momentum of a transition metal ion is quenched and the magnetic moment of transition metal ions results from the spin moment.

The fifteen rare earth elements extend from lanthanum (atomic number 57) to Lutetium (atomic number 71). The arrangement of their outer electrons is almost identical. The electron configuration for an isolated rare earth atom is $(Pd)^{46}4f^{n}\ 5s^{2}\ 5p^{6}\ 5d^{1}\ 6s^{2}$ where n is the number of electrons in the 4f shell. The number of electrons in the 4f shell varies from zero in La to 14 in Lu. The magnetic properties of the rare earths are due to this incomplete inner shell. The 4f electrons are shielded from the electric field of surrounding ions since they are so deep in the atom and unlike the transition metals their orbital moment is not quenched. In the elemental state and in alloys, rare-earth ions (with the exception of Eu and sometimes Ce) are trivalent.

2.2 Exchange Interaction

The coupling of magnetic moments in amorphous magnetic alloys is due to the exchange interaction and is usually written $H_i = \sum_{ij} J_{ij} \; S_i \cdot S_j$. The exchange strength depends on the distance between interacting atoms.

In transition metal alloys where the 3d shells overlap, the direct exchange interaction is the dominant interaction. It is considerably stronger than the RKKY interaction and it is a nearest neighbor interaction. Fig 2.1a shows the direct exchange interaction as a function of distance between interacting ions. The interaction strength depends on distance and there is the possibility of mixed ferromagnetic and antiferromagnetic interactions (i.e. exchange fluctuation). Since interatomic space is variable in amorphous alloys.

In rare earth alloys the indirect RKKY [16-18] exchange interaction is the dominant interaction and is responsible for magnetic ordering. The interaction has an oscillatory nature, (see fig 3b). A pair of magnetic ions chosen randomly will feel either a ferromagnetic or antiferromagnetic interaction depending upon their precise separation. The form of J (assuming a free electron) is shown in fig 2.1b where

$$J(r)=\mathrm{Cos}(2k_f r)/(k_f r)$$

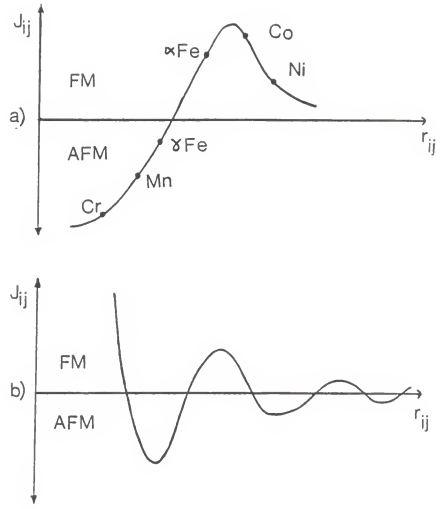

Figure 2.1 (a) The direct exchange interaction as a function of ion separation r_{ij} .
(b) The indirect [RKKY] exchange interaction as a function of ion separation r_{ij} .

This oscillation results from screening of magnetic ions by conduction electrons. Since the interatomic spacing of neighbouring ions varies in amorphous alloys the value of J between ion pairs also varies. In some cases both positive and negative values of J are possible, resulting in spatial fluctuation in exchange.

2.3 Random Magnetic Anisotropy Interaction

In the rare earths (non zero L) the origin of the strong random magnetic anisotropy is the strong random electric field gradients present in the alloys. The electrostatic interaction between the anisotropic charge of a rare-earth ion and the electric field gradient results in a random magnetic anisotropy which leads to an easy direction for the total moment of the ion. Since the electric field gradients are random, the easy direction will vary at random from site to site. In model systems random magnetic anisotropy is usually incorporated via a uniaxial energy term of the form $-D \sum_j (\hat{n}_i \cdot J_j)^2$ where D is the anisotropy strength and $\hat{n}$ is a unit vector describing the easy direction and varies at random from site to site.

In transition metals where the orbital angular momentum is quenched the random magnetic anisotropy is very weak.

2.4 Frustration

The variable nature of the exchange in amorphous alloys often introduces an element of conflict, called frustration, among the randomly positioned ions. A distribution of exchange interactions prevails due to the variable nearest neighbour distances. If this distribution is wide enough to encompass significant antiferromagnetic interactions, the ferromagnetic phase is unstable. The competition of ferromagnetic and antiferromagnetic coupling leads to an "ordered state" at sufficiently low temperature where the spins freeze in random directions. This state is the spin-glass state.

In the case of alloys with random magnetic anisotropy there is also a freezing in of the spins at low temperature much like a spin-glass. This state is referred to as a spin-glass state or speromagnetic state in the literature. Here we shall refer to it as a spin-glass state.

2.5 Spin Glass Models

Several models were proposed to treat the spin-glass problem. Sherrington and Kirkpatrick (SK)[8] considered an Ising spin model in which the spins are coupled by exchange interactions, with Gaussian probability density. The gaussian distribution for J_{ij} of width Δ which is centered about a value J_0 is given by

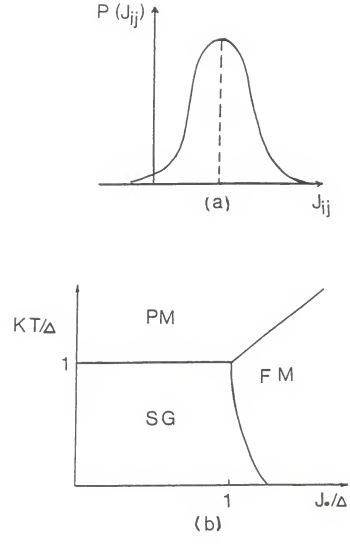

Figure 2.2 (a) The probability distribution of J_{ij} assumed in the Sherington-Kirckpatric model and (b) the derived magnetic phase diagram.

$$P(J_{ij})=[(2\pi)^{1/2}\Delta]^{-1}\exp[-(J_{ij}-Jo)^2/2\Delta^2]$$

and is illustrated in figure 2.2a.

In the (SK) model both spin-glass and ferromagnetic states can occur at low temperature. Fig 2.2b shows a schematic diagram of the (SK) model. The mean field assumption made in this model is not valid for real systems. In real magnetic systems only short-range interactions exist and Heisenberg models incorporating such interactions are not able to produce double transition behavior. They are able to produce PM-SG behavior provided a small anisotropy is included. The form of the anisotropy is not important with dipolar, Dzaloshinskii-Moriya and random magnetic anisotropy all producing similar SG behavior.

CH. III

EXPERIMENTAL METHODS

3.1 Preparation Of The Metallic Glasses

The systems which we studied for this thesis were in the form $Gd_{72-x}T_xGa_{18}B_{10}$, where T = Th, Al, Fe, Co, Mo, Pd and Er. The subscript numbers give the alloy composition in atomic %. To make an alloy the elements were first weighed according to the composition required. The elements were melted into a one gram polycrystalline button by using an arc furnace, fig 3.1a. The smaller pieces of metal were covered by the large pieces to stop the smaller pieces flying away during melting. The elements were melted in an argon atmosphere after pumping out the arc furnace chamber and flushing it three times with argon gas to minimize any oxidization during melting. The argon gas was allowed to flow continuously inside the champer during melting. An arc is produced by moving the tungsten electrode close to the copper anode and it was moved over the sample to get a homogeneous mixture. To get a better homogeneity the sample was turned over and remelted. The tungsten electrode is supplied with a current in the range 10-30 amp from a power supply to melt the compound. To avoid losing elements through evaporation, the elements melting time was about seven seconds. The mass loss for the alloys studied was less

than 0.1%.

In the case of the Th alloys some precautions, additional to those usually taken in alloy preparation, were required. The Th metal was in the form of a powder, and the arc furnace is used to melt the powder and form solid pieces of Th. During weighing and melting the powder we wore a mask and rubber gloves. We also worked late at night. Careful cleaning is required of the equipment and tools used to prepare the Th samples after preparation.

The splat cooling technique was used to prepare the amorphous alloys of this work and fig 3.1b shows a schematic diagram for this apparatus. A 300 mg piece of the button prepared previously by melting in the arc furnace was placed on the copper anvil and remelted in an argon atmosphere then squeezed between two cool surfaces which have come rapidly together. The current through the electrode is about 18 amp. It takes about one msec for the copper hammer to squeeze the alloy. The alloy temperature is decreased by about 1000 deg.Kelvin during this time so a cooling rate of approximatly 10^6 deg.K/s is obtained. The alloys obtained were in the form of circular discs about 3 cm in diameter and 50 μm thick.

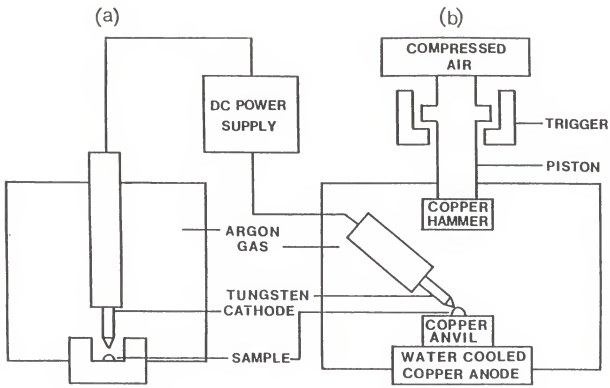

Figure 3.1 Schematic diagram of the (a) arc furnace apparatus.
(b) splat cooling apparatus.

3.2 Alloy Characterization

X-Ray diffraction was used to check the amorphousness of our alloys. Cu-K_α radiation is used and, the diffracted signal is detected by a proportional counter. The diffraction pattern observed for most alloys did not show any sharp crystalline diffraction peaks. For the Mo system x-ray diffractograms indicate the presence of small crystallization precipitates for the x = 24 at.% alloy it was estimated that 5-10% of the sample is crystalline. For the Fe system the alloys studied were amorphous except Fe x = 24 at.% alloy which was estimated to be about 2% crystalline.

3.3 Ac Susceptibility

The measured ac susceptibility is given by $X_{ac} = \partial M / \partial H_a$ where H is the applied field. The applied field is related to the internal field by

$$H = H_a - NM$$

where N is the demagnetization factor and depends on the geometry of the sample. The internal susceptibility $X = \partial M / \partial H$ is given by

$$1/X = 1/X_{ac} - N$$

which can be written as

$$X = X_{ac} / (1 - NX_{ac})$$

Thus, we expect

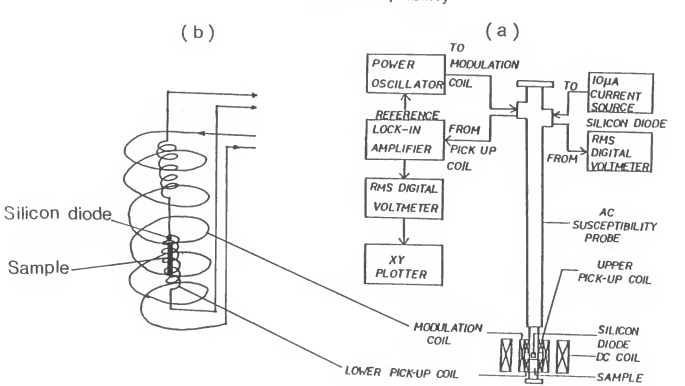

Figure 3.2 (a) Schematic of ac suceptibility apparatus.

(b) The two sets of coils in ac susceptibility probe.

$\lim X \longrightarrow \infty \quad ; \; X_{ac} \longrightarrow 1/N$

$\lim X \longrightarrow \text{small} \; ; \; X_{ac} \longrightarrow X$

The ac susceptibility apparatus is shown in fig 3.2a. Two sets of coils fig 3.2b are wound onto a derlin coil former. A set of modulation coils provide an ac field H=H coswt. The pick up coils which are wound in series opposition and are inside the modulation coil are used to detect the signal.

With no sample inside, the signal induced in the lower and upper halves of the pick up coil cancel, since they are wound in series opposition. With a sample inside the lower half of the pick-up coil the emfs become unbalanced and a signal is obtained. The signal is proportional to

$$dM/dT = (dM/dH_a)(dH_a/dT)$$

and after lock-in detection the induced signal is proportional to

$$\partial M/ \partial H_a$$

The temperature was measured using a silicon diode placed close to the sample. The voltage of the diode is recorded by digital voltmeter and an x-y plotter. The temperature of the sample is changed by raising and lowering the ac probe inside the He dewar. Temperature conversion from the diode voltage is provided by the

manufacturer. Samples used were in the form of strips weighing 30 mg, 0.8 cm long aligned with their long axis parallel to the applied field to reduce the demagnetization effects. The strips were inserted inside a plastic tube about 0.8 cm long and 0.2 cm in diameter.

3.4 Vibrating Sample Magnetometer (VSM)

The VSM technique is used to measure the dc magnetization. The VSM probe, (see fig 3.3), is vibrated mechanically at a frequency of 37 Hz. The sample is vibrated vertically between the centers of two pick-up coils in a constant magnetic field. The pick-up coils are wound in series opposition, and since the sample during vibration enters one half of the pick-up coil while leaving the other half, the emfs add. A lock-in analyzer is used to convert the output ac signal to a dc signal, which is monitored by a voltmeter and X-Y plotter. The dc signal is proportional to the magnetization and a standard sample is used to calibrate the system.

The temperature of the sample is measured by a silicon diode which placed near the sample at the end of the VSM probe. The temperature is changed by using a heater and the heater temperature is controlled using a Lake Shore Cryotronics temperature controller model 520, with a Ga-As diode in contact with the heater.

The sample used in magnetization measurement is the same as that used for ac susceptibility. The sample is aligned with its long axis parallel to the applied field to reduce the demagnetization effects.

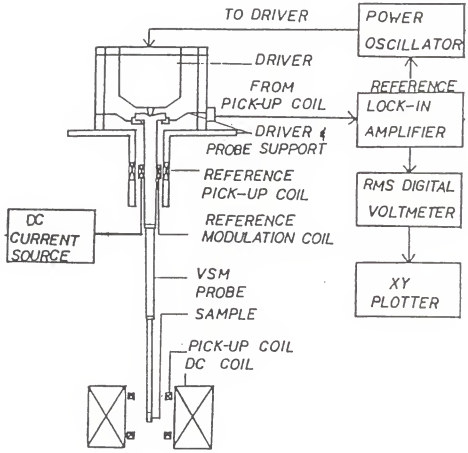

figure 3.3 Schematic of VSM apparatus.

3.5 The Torquemeter

The torque data of this work was taken on the capacitance torquemeter at Orsay, France by Dr. O'Shea and Dr. Fert who is on the physics faculty at Orsay.

The torque measurements are performed with a capacitance torquemeter fig 3.4. The sample is mounted on one of the plates of the capacitor, and is magnetized along the direction shown by cooling the sample in a horizontal applied field H_{fc} (field-cooling). H_{fc} is removed and a field H is then applied and rotated. The distance between the two plates is changed as a result of the torque on the sample and $\Gamma \alpha \Delta$. This changes the capacitance of the capacitor.

If H = 0, the capacitance is given by:

$$C_0 = (\epsilon_0 A)/d$$

For $H \neq 0$ $$C = (\epsilon_0 A)/(d+\Delta d)$$

so $$C = (\epsilon_0 A)/d(1+\Delta d/d) \approx C_0(1-\Delta d/d)$$

Note that the magnetic field is rotated in the plane of the sample and so for approximately circular foils the demagnetization field will not vary with direction.

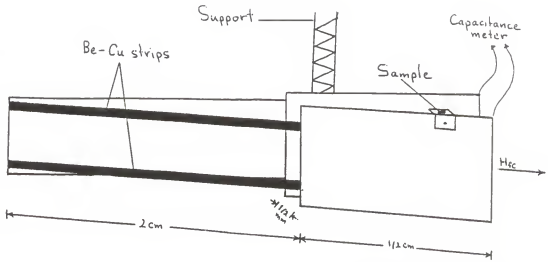

Figure 3.4 Schematic of capacitance torquemeter apparatus.

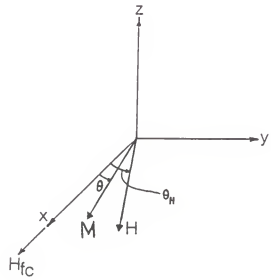

Figure 3.5 The field configuration in the torque experiment.

CH. IV

TORQUE MEASUREMENT

4.1 Introduction

The energy needed to rotate the spin system is known as the anisotropy energy $E(\theta)$, (θ is the rotation angle of M when the applied field is rotated through some angle θ_H), and is usually a rather a complicated function of θ.

In order to measure the torque $\Gamma = \partial E(\theta)/\partial\theta$, a field cooling technique is usually used to create a remanent magnetization M. The field cooling field is then removed, and a smaller field is applied (usually along the same direction), and then the field is rotated. The magnetization M rotates from its $\theta = 0$ direction when the magnetic field is rotated, and in general some irreversible spin rearrangement will occur at large enough angles. In terms of the magnetization M, which in general will also be a function of θ_H, the torque is given by

$$\Gamma = M(\theta)H\sin(\theta - \theta_H)$$

where θ and θ_H are the angles of rotation of M and H respectively as shown in fig 3.5.

4.2 Special Cases :

Case 1 : For systems with a large anisotropy, the magnetization M will remain frozen along the field cooling

direction as the applied field rotates,

$$M(\theta) = M(\text{constant})$$

$$\theta = 0$$

so $$\Gamma = MH\sin\theta_H$$

The torque vs. θ_H curve is (trivially) a reversible sine curve, fig 4.2a.

Case 2 : In the case of zero anisotropy the magnetization is able to follow the applied field and

$$\theta = \theta_H$$

so $$\Gamma = M(\theta)H\sin(0) = 0$$

Fig 4.2 b shows Γ vs. θ_H for this special case.

Case 3 : We now consider a more general case. A rigid rotation for the spin system may occur at small angles, At large enough angles irreversible rearrangement of the spins will take place. As the magnetic field is rotated further, a steady state will be reached where the angle between M and H is constant, and M does not vary in magnitude. In this regime Γ will be a constant. When the rotation is reversed the torque changes sign as M crosses H and a steady state is again reached, see fig 4.2c.

Case 4 : Finally a last case we will consider is where there is a special anisotropy direction in the alloy. A possible example could be a crystal where the magnetization has an easy axis along a particular

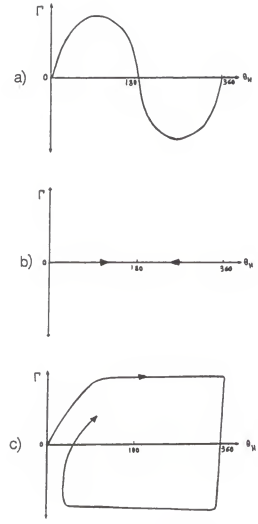

Figure 4.1 The torque vs. θ_H for the special cases:
(a) system with large anisotropy.
(b) system with zero anisotropy.
(c) system with no special anisotropy direction.

crystalline direction and a hard direction perpendicular to it. The torque will show a maximum as M pulled through the hard direction and a minimum as it goes through the easy direction.

4.3 Experimental Results

Torque measurement have been made for the $Gd_{72}Ga_{18}B_{10}$ sample on which the alloys of this work are based. Fig 4.3 shows the effects of applying the field-cooling field of 8 kOe along θ=0 and -90. As can be seen, a rather complicated torque curve is obtained. The main point to note is that the structure occurs at the same value of θ_H for different initial field-cooling angles indicating that the sample has a fixed anisotropy. The peaks correspond to the situation where the applied field pulls the magnetization through a hard direction. These results indicated that there exist macroscopic easy and hard directions in this alloy and show that there is probably some crystalline order undetected in x-rays in the alloy. We do not however find any difference in ac susceptibility for alloys where the ac field is applied along different directions and we discuss these results in the next chapter.

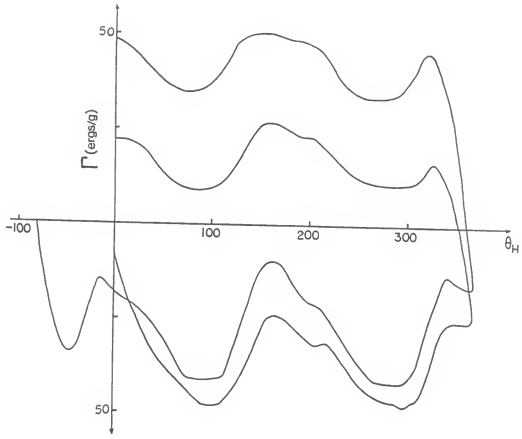

Figure 4.2 The torque vs. θ_H for the $Gd_{72}Ga_{18}B_{10}$ sample at H=1 kOe and T=4.2 K for different field-cooling angles.

CH. V

AC SUSCEPTIBILITY AND THE MAGNETIC PHASE DIAGRAM

5.1 Introduction

The ac susceptibility was measured by using the apparatus shown in fig (6a). The ac susceptibility for our standard reference alloy $Gd_{72}Ga_{18}B_{10}$ is shown in fig 5.1. It shows a rapid rise at the ferromagnetic transition temperature. It approaches the demagnetization limit and remains at this value until the ac susceptibility drops off as the spin-glass phase is entered.

The paramagnetic-ferromagnetic transition temperature T_{pf} is determined from the steepest portion of the initial rise with decreasing temperature of the ac susceptibility curve and the ferromagnetic-Spin-glass transition temperature T_{fg} is determined Fom the steepest portion of the downturn of the ac susceptibility curve. In case of a PM-SG transition, the transition temperature T_{pf} is determined from the peak position of the ac susceptibility.

In the previous chapter we showed that an in-plane anisotropy exists in $Gd_{72}Ga_{18}B_{10}$ and it is probably due to some crystalline order undetected in x-rays. We have done ac susceptibility on $Gd_{72}Ga_{18}B_{10}$ with the ac field directed along different directions, and we find no

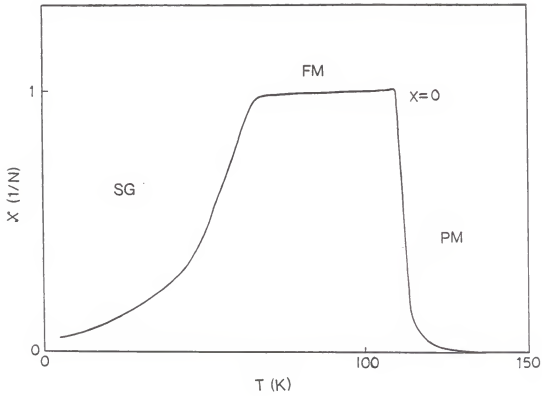

Figure 5.1 Ac susceptibility of the $Gd_{72} Ga_{18} B_{10}$ alloy.

changes in the transitions observed.

The magnetic phase diagram of each series of alloys is determined from the results of ac susceptibility where the transition temperature vs. composition (x at.%) is plotted. Fig 5.2 shows the magnetic phase diagram of the systems Gd-Mn and Gd-Ni[15] done by Jantan and to which we will compare our results. As seen from the magnetic phase diagram the two systems show double-transition behavior. The multicritical point (the composition at which the system changes behavior from double transition to single transition behavior) of the Gd-Mn system is at about 33 at.% Mn.

5.2 Th system

The Th system shows behavior similar to the La system. Fig 5.3a shows the ac susceptibility and fig 5.3b shows the magnetic phase diagram deduced from it. A cross-over to paramagnetic-spin-glass behavior occurrs close to x=7 at.%. For x < 6 double transition behavior is observed. The transition temperatures T_{pl} and T_{lg} are observed to decrease and increase respectively with an increase in x. For x > 6 at.% a single peak with a maximum below the demagnetization limit is present and is a characteristic of a PM-SG transition. The disappearance of the double transition behavior is believed to be

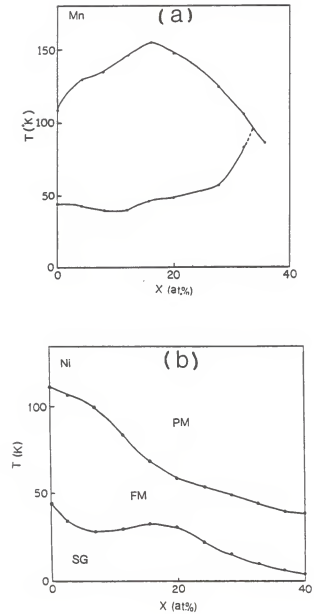

Figure 5.2 The magnetic phase diagram of the (a) Gd-Mn system. (b) Gd-Ni system.

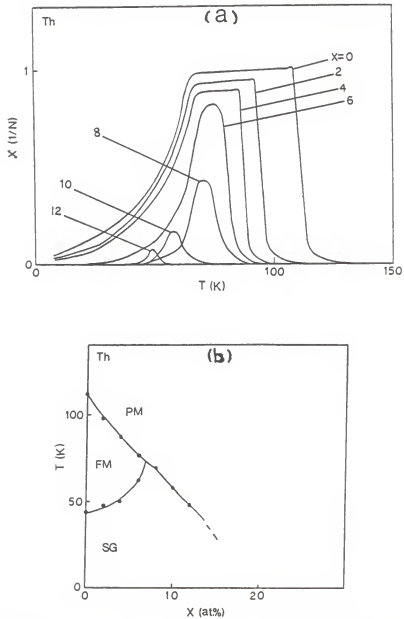

Figure 5.3 (a) Ac susceptibility of the Th system.
(b) The magnetic phase diagram of the Th system.

related to an increase in exchange fluctuation as the Th content is increased resulting in increased frustration effects in the system. The x = 6 at.% alloy shows a broad peak close to the demagnetization limit and it is likely that double transition behavior exist in this alloy as was found earlier for double transition alloys of the La system [2], where the ac susceptibility shows a broad peak with a maximum just below the demagnetization limit.

5.3 Al System

The ac susceptibility of the Al system is shown in fig 5.4a, and the magnetic phase diagram is shown in fig 5.4b. Double transition behavior is present for the alloys with $x \leqslant 12$ at.% Al. Single transition behavior is observed for alloys with $x \geqslant 16$ at.% Al. It is shown clearly from the phase diagram that the ferromagnetic ordering temperature T_{0f} and the spin-glass ordering temperature T_{fg} are decreased and increased respectively with increasing the value of x. A multicritical point is present for the Al system at $\simeq$ 14 at.%, and is at a considerably higher value than for the La and Th systems.

5.4 Fe System

The ac susceptibility results of the Fe system are shown in fig 5.5a and the magnetic phase diagram is shown in fig 5.5b. The effect of Fe is to destroy the spin-glass

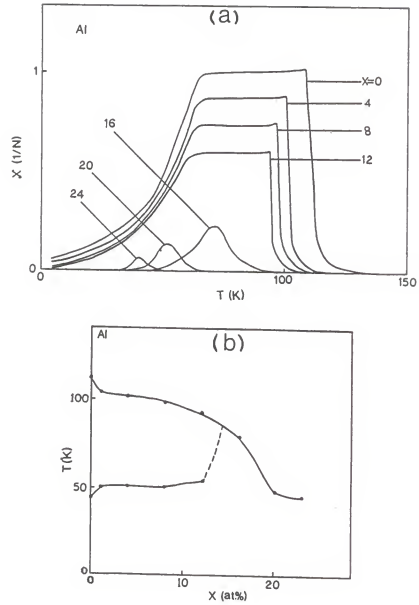

Figure 5.4 (a) Ac susceptibility of the Al system.
(b) The magnetic phase diagram of the Al system.

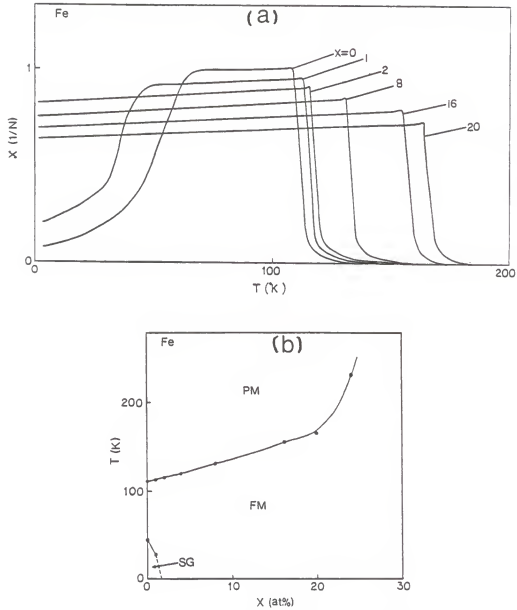

Figure 5.5 (a) Ac susceptibility of the Fe system.
(b) The magnetic phase diagram of the Fe system.

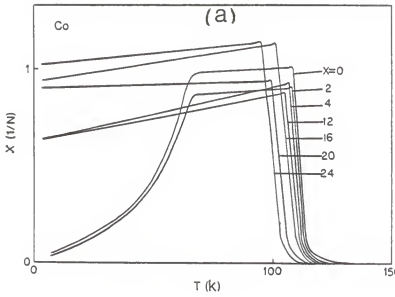

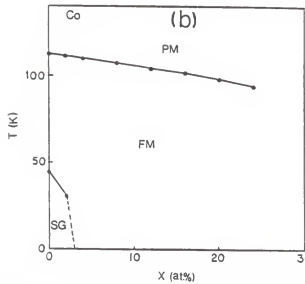

Figure 5.6 (a) Ac susceptibility of the Co system.

(b) The magnetic phase diagram of the Co system.

behavior for small values of x (x > 1). The ferromagnetic ordering temperature rapidly increases with increasing values of x. These effects indicate that alloying with Fe significantly increases the ferromagnetic exchange.

5.5 Co System

Fig 5.6a shows the ac susceptibility results and the magnetic phase diagram is shown in fig 5.6b. Alloying with Co leads to the destruction of the spin-glass behavior, but in contrast to Fe, Co produces a small decrease in the transition temperature.

5.6 Pd System

In case of the Pd system the ac susceptibility shows that double-transition behavior exist for the alloys with $x \leqslant 12$ at.% Pd fig 5.7a. A single transition is observed for the alloys with composition x = 16, and 18 at.%. With increasing Pd content the transition temperature T_{pf} is slightly decreased. From the ac susceptibility results we note that the frustration effects become stronger with increasing x. A multicritical point is present at about 14 at.% as may be seen from the phase diagram in fig 5.7b. This value is similar to that of the Al system but much higher than those of the La and Th systems.

5.7 Mo System

Fig 5.8a shows the ac susceptibility of the Mo

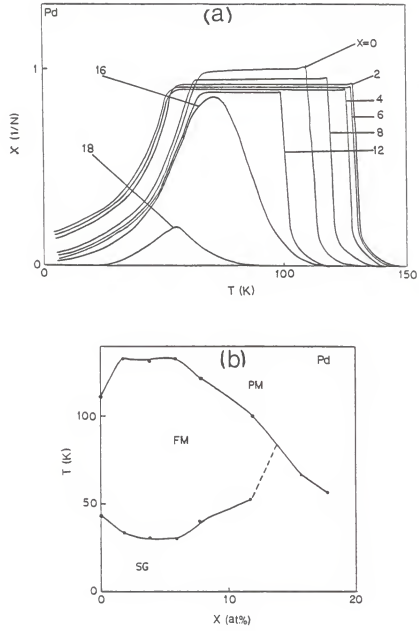

Figyre 5.7 (a) Ac susceptibility of the Pd system.
(b) The magnetic phase diagram of the Pd system.

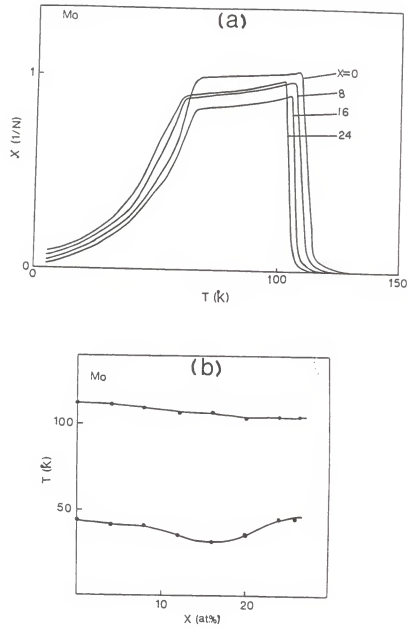

Figure 5.8 (a) Ac susceptibility of the Mo system.
(b) The magnetic phase diagram of the Mo system.

system. The ac susceptibility measurements indicate surprisingly little change in the double-transition behavior up to x = 24 at.% Mo, the highest concentration studied, as may be seen from fig 5.8b. The transition temperature T_{pf} is decreased a little as the value of x increased. The transition temperatures for the Mo system are summarized in the magnetic phase diagram shown in fig 5.8b. No multicritical point is found for this system. A small amount of crystallinity is present in the x=24 at.% Mo alloy, but this crystallinity does not appear to produce any significant changes in ac susceptibility as compared to Mo alloys with smaller x.

5.8 Er System

The results of the ac susceptibility are shown in fig 5.9a and the magnetic phase diagram is shown in fig 5.9b. The Er system shows double transition behavior for alloys with $x \leqslant 10$ at.% Er. A single transition is observed for alloys with $x \geqslant 12$ at.% Er. The magnetic phase diagram shows regions of paramagnetic, ferromagnetic and spin-glass behavior. A multicritical point exists at about x = 11 at.% as shown in the magnetic phase diagram, and it is shown clearly that for x > 11 at.% a single transition behavior is present.

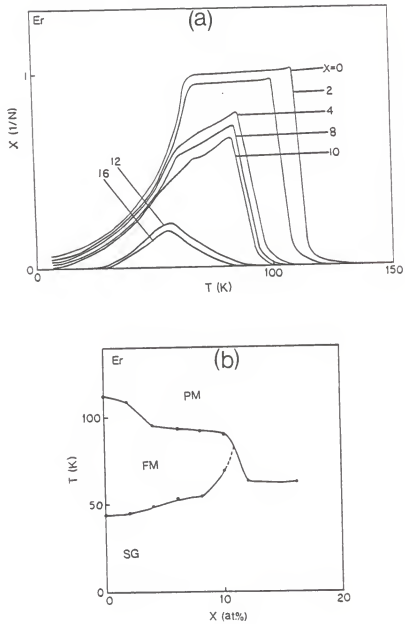

Figure 5.9 (a) Ac susceptibility of the Er system.
(b) The magnetic phase diagram of the Er system.

CH. VI

MAGNETIZATION MEASUREMENTS

High field measurements were made at 4.2 K for selected systems. We chose the Th (Fig 6.1), Al (Fig 6.2), Fe (Fig 6.3), and Er (Fig 6.4). These elements were selected because their properties differ as follows. Both Th and Al are nonmagnetic but they have different atomic radii which lead to different types of short-range order resulting in the somewhat different phase diagrams (chap. V). Fe and Er both carry a moment, and in addition Er incorporate a significant anisotropy. The high field magnetization and coercivity are summarized in figures 6.5 and 6.6 respectively.

In the case of the Fe system the magnetization saturates in low fields for all alloys studied and the coercivity decreases significantly to values < 70 Oe for x > 4 at.%. The saturation of magnetization in low fields shows that alloying with Fe decreases the frustration effects in this system.

All the Th and Al alloys show curvature in their magnetic isotherms at high fields. For x > 4 at.% the magnetization at high fields (75 kOe) is far from saturation indicating the presence of strong frustration effects. An increase in coercivity is also observed with

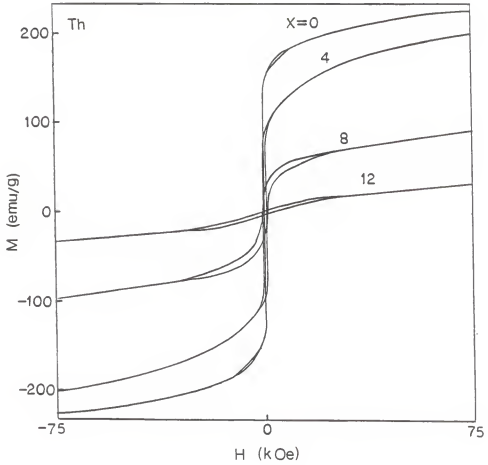

Figure 6.1 Hysteresis loops for selected Th alloys.

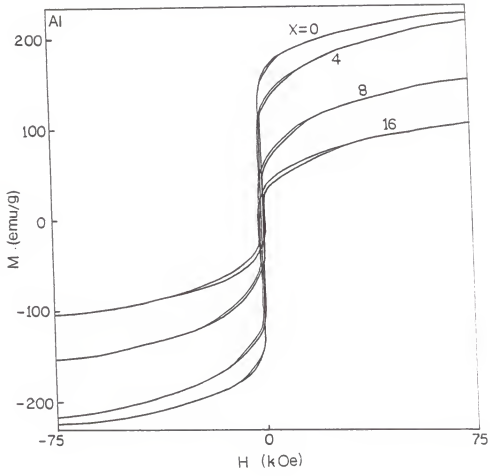

Figure 6.2 Hysteresis loops for selected Al alloys.

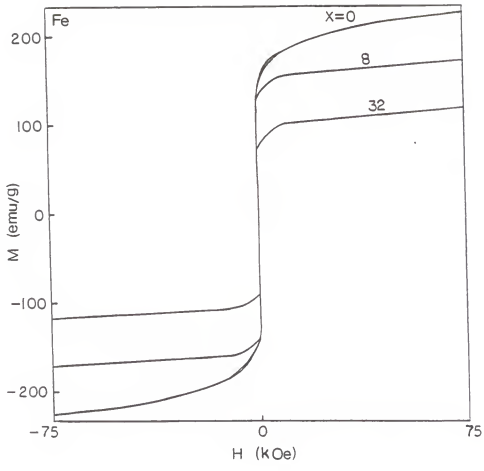

Figure 6.3 Hysteresis loops for selected Fe alloys.

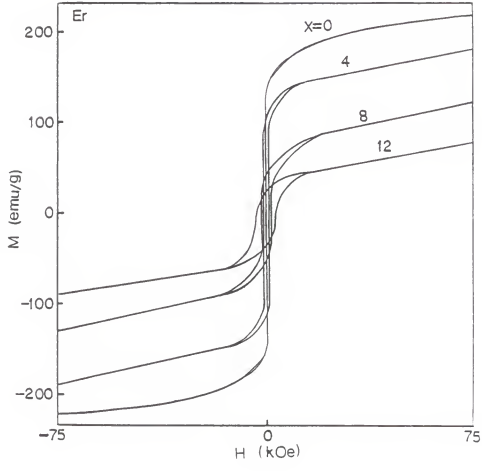

Figure 6.4 Hysteresis loops for selected Er alloys.

increasing Th or Al content as shown in fig 6.6.

For the Er system, the coercive field shows a gradual increase with increasing values of x , reaching a value of 2.85 kOe for the x = 16 at.% Er alloy. This is the largest coercivity of all the alloys at x = 16 at.%. Also it becomes increasingly difficult to saturate the magnetization as the Er concentration increases.

All the SG alloys measured show a dependence of M on time. This effect has been seen in many other spin-glasses and has been found to be logarithmic in nature with

$$M = M - S(T)\ln\log(t-t_0) \qquad (1)$$

describing the dependence of M on time after cycling the applied field to a high value (in our case 55 kOe) and back to zero. The time t is the time between decreasing the field to zero and making the first measurement. t_0 is only known to the nearest 30 seconds since the superconducting power supply takes approximatly this long to shut off after reaching zero field. This time dependence of M in the SG phase shows the strong nonequilibirium effects present in the SG phase.

Figure 6.7a shows M vs $\log(t-t_0)$ and the linear behavior indicates that magnetization as a function of time conforms well to equation (1) for times up to

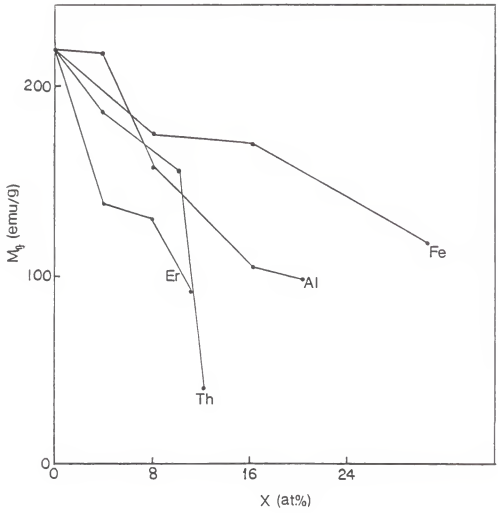

Figure 6.5 Saturation magnetization M_0 as a function of composition for the Th, Al, Fe, and Er systems.

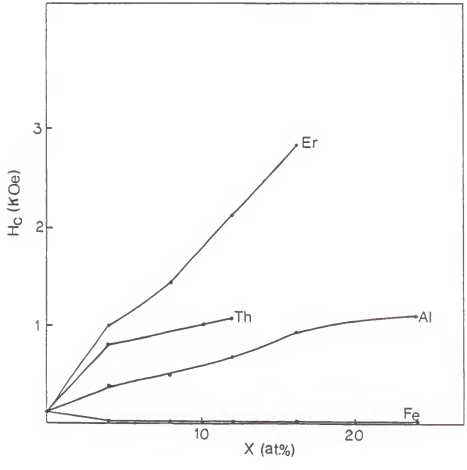

Figure 6.6 Coercivity H_c as a function of composition x for the Th, Al, Fe, and Er systems.

13 minutes. Figure 6.7b shows the dependence of S on temperature and it has a peak at intermediate temperatures and goes to zero before the FM-SG transition is reached (T_{fg} = 44 K). This behavior is characteristic of alloys with a SG phase.

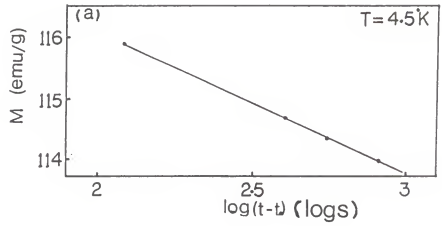

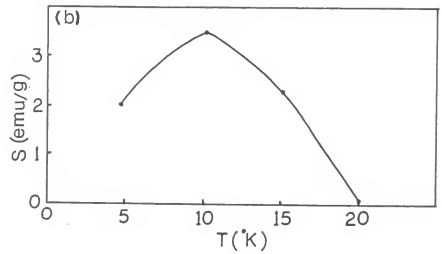

Figure 6.7 (a) M vs. Log $(t-t_0)$ for $Gd_{72}Ga_{18}B_{10}$ alloy at 4.5 K.

(b) S vs. T for $Gd_{72}Ga_{18}B_{10}$ alloy.

CH. VII

DISCUSION AND CONCLUSION

7.1 Discussion

We have reported here the effect of alloying both magnetic and nonmagnetic elements on the double-transition behavior of Gd-rich spin-glass systems. In our work we kept the glass-forming components ($Ga_{18}B_{10}$) identical. This enables us to study the alloying effects independent of changes induced by the addition of metalloids needed for glass formation. We have summarized the main results from chapter V and VI in table 1.

7.1.1 Effects of short range order

In all amorphous systems there is some short-range structural order. The results of the torque measurments show that the short-range order in the $Gd_{72}Ga_{18}B_{10}$ alloy is anisotropic in nature since it has macroscopic easy and hard directions. This anisotropy does not appear to effect the ac susceptibility since there were systematic variations in (1) the magnitude of the ac susceptibility and (2) transition temperature as determined from the maximum slope or peak position in ac susceptibility with composition x when the samples chosen were randomly oriented.

The magnetic phase diagram of the Th system is

similar to that of the Gd-La system with the La and Th systems having multicritical points at 6 and 7 at.% respectively. In general both structural short-range order (present to some extent in all amorphous systems), and electronic structure may vary upon alloying. The similarity of the La and Th magnetic phase diagrams indicate that both elements act similarly. This is not surprising since both have similar atomic radii, (see table 2), and a valence of 3 (as does Gd). The phase diagram for these systems can be understood on a qualitative level. Nearest neighbour Gd-Gd interactions tend to be ferromagnetic. For example pure Gd has a ferromagnetic transition at 293 K. The effect of the alloying is then to remove nearest neighbour Gd pairs and so decrease the ferromagnetic exchange.

The Al and Pd systems have multicritical points at x 14 at.%. Judging from the magnetic phase diagrams one can conclude that increasing the Al and Pd content will increase the exchange fluctuations leading to a frustration in the system. The Al and Pd ions have a significantly smaller atomic radius than the Gd, and the short-range order is, therfore likely to differ from the La and Th alloys. We believe that this is the main reason for the difference in the phase diagrams.

The effects of the exchange fluctuations were seen in the slow approach of magnetization to saturation in the above alloys.

The above comparison of the Al and Pd systems with the La and Th systems shows that short-range order is important in determining the microscopic interactions in these alloys. But we note that in all of the systems (with the exception of Ni) were a non-magnetic element was alloyed into $Gd_{72}G_{28}$ a cross-over to PM-SG transition behavior eventually occured.

7.1.2 Effects of magnetic elements

Alloying with Fe or Co leads to a destruction of the spin-glass phase. The results of ac suscebtibility indicate that a strong ferromagnetic exchange is present in the Fe-rich alloys. In contrast to the Fe system, the Co system shows a small decrease in ferromagnetic ordering temperature and this probably results from a strong antiferromagnetic Gd-Co interaction. Co is known to be antiparallel to Gd in amorphous alloys (e.g. $Gd_{65}Co_{35}$) [19]. Fe is also known to be coupled antiferromagnetically with Gd but the frustration effects produced by Fe do not appear to be as strong [19]. These frustration effects at large x are apparently either not strong enough or not of the right form to reintroduce the spin-glass behavior.

Related studies in the Ni system done by Jantan, show that the FM-SG transition appears to vanish but at a larger value of x than for the Co and Fe systems. The FM-SG transition temperature goes to zero at an extrapolated value of x = 48 ∓ 2 at.% [20]. This indicates that the addition of Ni does not increase the exchange fluctuations. This is also shown in the results of the high field magnetization, with alloys with higher Fe (this work) or Ni [20] content tending to saturate in lower fields .

Studies done by Jantan in the Mn system show that alloying with Mn increases the exchange fluctuations leading to a cross-over from double transition to single transition behavior. Amorphous Gd-Mn alloys have been shown to have a strong antiferromagnetic Gd-Mn interactions. These strong antiferromagnetic interactions results in a slow approach to saturation at high magnetic fields.

7.1.3 Effects of an immisible element

For the Mo system, increasing x does not effect the double-transition behavior significantly. The double-transition behavior exists for all the samples studied and $T_{}$ and $T_{}$ are nearly constant (there is a small dip in T_{fg}). Mo is not miscible in Gd and so it is likely that a two phase system is formed in our samples which have regions

rich in Mo and other regions rich in Gd-Ga-B.

7.1.4 Effects of anisotropy

For the Er system double-transition behavior exist for alloys with x < 10 at.% Er. Single transition behavior is observed for the samples with x > 12 at.% Er. A multicritical point exists for the Er system at about x = 11 at.% Er. Er is known to couple ferromagnetically to Gd and so the frustration effects here are due to the random magnetic anisotropy incorporated by the Er.

A number of studies have been done in alloys with exchange fluctuations and alloys with random magnetic anisotropy and it is known that a strong coercivity results from random magnetic anisotropy rather than fluctuations in exchange. This result is clearly seen here with Er (even though the random magnetic anisotropy is not very strong) producing the largest increase in coercivity.

From the magnetization measurment results, no saturation is reached at high fields (75 kOe) for any of the alloys showing a PM-SG transition. This result indicates that strong frustration effects exist in these systems. In the Fe system where PM-FM behavior only is present for large Fe content, saturation of the magnetization is obtained in fairly low fields as one

would expect since frustration effects are small.

7.2 Conclusion

We have studied the effect of alloying magnetic (Fe, Co, Mn, and Er) and non-magnetic (La, Al, Th, Mo, and Pd) elements on the double-transition behavior of $Gd_{72}Ga_{18}B_{10}$. Of these elements only Er incorporates a significant anisotropy.

High field Magnetization measurments indicate that frustration effects exists in all the alloys studied which show PM-SG transition behavior.

The La and Th systems show similar magnetic phase diagrams to each other since their ionic radii are nearly equal to that of Gd. Th and La have multicritical points at values of x of about 7 and 6 at.%. Al and Pd show multicritical points at a value of x of about 14 at.%. They have similar ionic radii but are somewhat smaller than Th, La, or Gd. As the value of x is varied changes in the short-range order occur since Al and Pd have smaller ionic radii than Gd and we believe this is the reason why their phase diagrams differ from those of Th and La.

Alloying with Fe or Co leads to a destruction of the spin-glass behavior. Strong ferromagnetic exchange exists

in these systems. Similar behavior was observed for the Ni system but much higher Ni concentrations were needed to destroy the spin-glass behavior.

We also studied the effect of alloying with an element which incorporates a random magnetic anisotropy (Er). Double transition behavior still exists for the values of $x < 10$ at.% and single transition behavior for $x > 12$ at.%. And so the frustration introduced by the random magnetic anisotropy leads to destruction of the double-transition behavior in a similar way to exchange fluctuations. The largest increase in coercivity was observed for the Er system as expected since Er incorporates a significant random magnetic anisotropy.

Mo shows a surprising magnetic phase diagram. The PM-FM and FM-SG phase boundaries are nearlly parallel. A dip is present in the FM-SG boundary at intermediate values of x. Since Mo is not miscible in rare-earths (to more than about 2%) a two-phase system probably exists here.

Table 1 summarizes the results we obtained from the ac susceptibility, magnetization and x-ray measurments.

Element	Crystallinety detected	Brittle for	Multicritical point	Coercivity X=12 at.%	Approach to saturation	Initial increase in T
Al	none (x<16 at.%)	x>16 at.%	13 at. %	0.68 kOe	slow	No
La [2]	none (x<72 at.%)	none	5 at. %	-	slow	No
Fe	x>24 at. %	x>20 at.%	none	70 Oe	fast	Yes
Co	none (x<24 at.%)	none	none	70 Oe	fast	No
Ni [15]	x>34 at. %	x>24 at.%	none	-	fast	No
Mn [15]	x>34 at.%	x>24 at.%	33 at. %	-	slow	Yes
Pd	none (x<18 at.%)	x>16 at.%	13 at. %	-	-	Yes
Mo	x>24 at. %	x>20 at.%	none	-	-	No
Er	none (x<18 at.%)	x>12 at.%	11 at. %	2.21 kOe	slow	No
Th	none (x<12 at.%)	none	7 at. %		slow	No

Table 1: Summary of experimental results

Element	Gd	La	Th	Al	Pd	Fe	Co	Mo	Er
	1.61	1.69	1.65	1.18	1.28	1.17	1.16	1.30	1.57

Table 2: Ionic radii in angstroms

REFERENCES

1. Y. Yeshurum, M. B. Salamon, K. V. Rao and H. S. Chen, Phys. Rev. B 24, 1536 (1981).
2. M. J. O'shea, D. J. Selmyer, Phys.Rev. B32, 7502, (1985).
3. J. Lauer, and W. Keune, Phys. Rev. Lett. 48, 1850 (1982).
4. G. A. Gist et. al.. Phys. Rev. B 34, 1683 (1986).
5. R. Rammel and J. Souletie, in Magnetism Of Metals and Alloys, edited by M.Cyrot (North-Holland, Amsterdam, (1982).
6. Peter J. Ford, Contemp. Phys. 23, 141 (1981).
7. R. W. Walstedt and L. R. Walker, Phys. Rev. Lett. 47, 1624 (1981).
8. D. Sherrington and S. Kirkpatrick, Phys. Rev. Lett. 35, 1792 (1975).
9. C. M. Soukoulis, K. Levin, and G. S. Grest, Phys. Rev. B 28, 1510 (1983).
10. M. J. O'Shea. K. M. Lee, and F. Othman, Phys. Rev. B 34, 4944 (1986).
11. J. M. D. Coey, J. Appl. Phys., 49, 1646 (1978).
12. J. A. Gerber, D. J. Miller, and D. J. Sellmyer, J. Appl. Phys. 49, 1699 (1978).
13. M. J. O'Shea, and D. J. Sellmyer. J. Appl. Phys., 53, 7722 (1982).

14. M. J. O'Shea, and D. J. Sellmyer. J. Appl. Phys. 57, 3470 (1985).
15. Jafar Jantan, Master Thesis, Kansas State University, 1985.
16. M. A. Ruderman and C. Kittel, Phys.Rev.Lett. 96, 95 (1954).
17. K. Yosida, Phys.Rev.Lett. 106, 893 (1957).
18. T. Kasuya, Prog.Ther.Phys. 16, 45 (1956).
19. K. Moorjani, and J.M.D. Coey, Methods and phenomena 6 Magnetic Glasses, 1984.
20. M. J. O'Shea, and Jafar Jantan. To be published.

MAGNETIC BEHAVIOR OF Gd-RICH SPIN-GLASS SYSTEM

by

ABDEL-LATIF AL-SHARIF
B.Sc., YARMOUK UNIVERSITY-JORDAN, 1984

AN ABSTRACT OF A MASTER'S THESIS
submitted in partial fulfillment of the
requirement for the degree
MASTER OF SCIENCE

Department of physics
KANSAS STATE UNIVERSITY
Manhattan, Kansas
1988

ABSTRACT

We investigated the effect of alloying a number of elements on the magnet double-transition behavior of $Gd_{72}G_{28}$ (G_{28}=Ga_{18} B_{10}). The alloys are prepared by the splat cooling technique and have composition $Gd_{72-X}T_XG_{28}$ where T = Th, Al, Fe, Co, Pd, Mo and Er. Torque, ac susceptibility and magnetization measurments were used to study these alloys. The purpose is to gain a better understanding of the double-transition and spin-glass transition behavior seen in many amorphous alloys.

X-rays do not shown any sign of crystallinity in most of the alloys but torque measurments show that our samples are not completly amorphous. The short-range order in them leads to easy and hard macroscopic directions. Alloying with Th, La, Al or Pd produce a cross-over from the double-transition behavior of $Gd_{72}Ga_{18}B_{10}$ to paramagnetic-spin-glass transition behavior due to the increase in exchange fluctuations and some clear effects on the size of the element which we believe are related to short-range order are seen. Alloying with Fe or Co destroys the spin-glass behavior.

Alloying with Mo does not effect the double-transition behavior most likely because the alloys with Mo

are phase separated into Mo-rich and Gd-Ga-B rich phases.

Finally alloying with Er which incorporates random magnetic anisotropy leads to a rapid cross-over to paramagnetic-spin-glass behavior similar to what is seen when the strength of exchange fluctuation are increased.